Buckling induced by dilative strain in two- and three-dimensional layered materials

Sherwin J. Singer
Department of Chemistry, Ohio State University, Columbus, Ohio 43210
(Received 30 March 2000)

Buckling of stripes in two dimensions, or layers in three dimensions, induced by dilative strain, is observed in thin films, in liquid crystals, and at interfaces. Equations for the buckling pattern are analyzed and solved in this work. We have previously predicted buckling patterns in two-dimensional systems, which were subsequently successfully compared with experiment. Here we make predicted buckling profiles for three-dimensional layered materials available for comparison with experiment. We also analyze dilative strain-induced buckling on a qualitative level, in terms of mechanical analogy, and compare the modulation pattern with that which arises in other contexts.

PACS number(s): 61.30.−v, 83.70.Jr, 47.20.Ma, 87.16.Dg

Layered materials, such as stripe phases in two-dimensional Langmuir layers or thin magnetic films, or three-dimensional smectic phases, are host to a multitude of phenomena whose detailed understanding is both scientifically challenging and technologically significant. In this work we study periodic buckling in response to dilative strain, which occurs in a wide variety of layered materials. Control of this effect in smectics is relevant to the design of liquid crystal displays [1–11]. We provide new results on the buckling pattern beyond the limit where it can be described by one Fourier mode or a few. Buckling patterns beyond the single-mode limit for three-dimensional materials like smectics are calculated for the first time in this work, to our knowledge.

Dilative strain favors uniform tilting of the layers because the perpendicular spacing between layers tilted by an angle θ is reduced by a factor of $\cos\theta$, as shown in Fig. 1, and the spacing thereby approaches the equilibrium spacing before the onset of strain. If it were possible for uniformly dilated layers to tilt with no other associated energy costs, they could return to equilibrium by this path. The new equilibrium state would be tilted by an angle $\theta=\cos^{-1}(1/(1+\alpha))$ in the presence of dilative strain α. As a *periodic* buckling pattern, overall tilting can be classified as a zigzag or chevron pattern of infinitely large wavelength. However, boundary constraints thwart simple tilting as a route to equilibrium. For example, in the case of smectics held between plates parallel to the layers, the plates impose a boundary constraint that resists tilting and excludes a complete return to equilibrium by over all tilting or infinite wavelength zigzags. Now the buckling pattern is selected by a competition between strain release by layer tilting and the resistance at the boundaries. In other systems, such as magnetic stripe phases, less controllable factors like pinning defects provide the resistance that frustrates overall tilting.

Strain-induced periodic buckling has been observed in two-dimensional magnetic stripe phases [12–15], ferrofluids [16], and in three-dimensional smectic-*A* liquid crystals [1,17]. Modulations along both one and two directions were observed in experiments on smectics [1]. The effect in chiral ferroelectric smectics [2–11] is particularly important, since the response of these materials is exploited in the construction of new liquid crystal displays. Strain-induced periodic buckling was also observed in a columnar liquid crystal [18]. Our previously calculated buckling profiles [19] modulated along a single direction, have been successfully compared with experiments for both chiral ferroelectric smectics [20] and columnar liquid crystals [18]. The transition from sinusoidal layer undulation near the buckling threshold to a chevron pattern with increasing strain was predicted in our previous work [19], and confirmed experimentally [20]. In this work we predict fully three-dimensional patterns, including a three-dimensional analog of the transition from sinusoidal to chevron buckling, that will hopefully be tested against experiment as well.

The threshold condition for dilative strain-induced layer buckling was derived by Clark and Meyer [21], assuming a single Fourier mode buckling pattern at threshold, a result which is unaffected by our more extensive analysis. Since the continuum free energies under an applied electromagnetic field or under dilative strain are identical to second order in the elastic displacement field, provided the proper transcription is made between coupling constants in the two cases, the threshold laws are analogous to those previously derived by Helfrich [22,23] and Hurault [24] for layered materials (cholesterics) in electromagnetic fields. Delrieu [25] gave the critical strain for a fully three-dimensional situation, that is, for buckling patterns described by two or three noncoincident wave vectors of equal magnitude. Wang treated dilative strain of a lamellar phase, but his treatment was also restricted to a single Fourier mode buckling pattern [26].

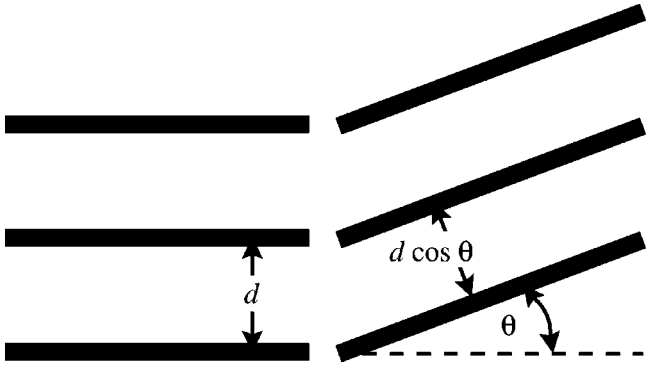

FIG. 1. Reduction of perpendicular layer spacing from d to $d\cos\theta$ upon overall layer tilting.

Buckling patterns beyond the single Fourier mode limit at threshold were previously treated for only two-dimensional systems, that is, for layers modulated along a single direction. Nakagawa developed a soliton theory for chevron kinks [27]. Pavel and Glogarová derived expressions for buckling patterns which, like those of Nakagawa, are only valid in the chevron limit [28]. This was followed by derivations of buckling patterns valid from threshold to the chevron limit by this author [19] and by Limat and Prost [29]. Kralj and Sluckin examined the transition from sinusoidal to chevron structure in smectic-*A* liquid crystals confined between parallel plates in the so-called bookshelf structure [30], treating the system as two dimensional. Their calculation separately tracked both the molecular director and the layer density, more cumbersome than our formulation but furnishing more detailed information. A similar study for chevron formation upon the smectic-*A* to smectic-*C* transition was performed by Vaupotic *et al.* [31]. Stewart studied the related problem of layer undulation caused by magnetic fields in smectics [32]. His analysis was specific to finite samples, in contrast to our treatment of systems, which are finite perpendicular to the layers and infinite parallel to the layers. As discussed below, Stewart neglected terms in the elastic free energy which, in the dilative strain case, are crucial to describe the transition from sinusoidal to chevron buckling patterns with increasing strain.

A similar treatment of stripe buckling, this time in the context of stripe domains in liquid crystalline elastomers, was independently derived a few years later by Finkelmann *et al.* [33]. Layer buckling in smectic elastomers is a more complicated problem, because it involves coupling between the smectic layer displacements and other elastic variables. It was treated by Weilepp and Brand in the single Fourier mode limit [34]. Read *et al.* studied the two-dimensional transition from sinusoidal to chevron buckling patterns in smectic elastomers using numerical finite element modelling [35]. The variational scheme introduced in this work should enable full three-dimensional studies of layer buckling in elastomers.

Besides extending the treatment of layer buckling to the full three-dimensional case, in Sec. I we develop a qualitative picture of the origins of strain-induced buckling using a mechanical analogy. Using this formalism, we contrast the factors governing buckling via dilative strain to another situation, buckling of a monolayer in response to compression [36]. The qualitatively different buckling patterns can be understood in terms of the effective potential of the mechanical analogy. In Secs. II–IV, the equations for full three-dimensional layer buckling are simplified. Results for two- and three-dimensional buckling patterns are given in Sec. V.

I. A MECHANICAL ANALOGY AND COMPARISON TO BUCKLING IN ANOTHER CONTEXT

Before presenting detailed results, it is worthwhile to explore the qualitative features of equations governing buckling patterns. For the purpose of this discussion, we work in the relative simplicity of buckling along a single direction. We also postpone consideration of boundary conditions in the direction perpendicular to the layers, the Z direction, and furthermore suppose that the system is changing slowly in this direction. (All of these restrictions are relaxed below.) This leaves us with one-dimensional equations which can be qualitatively interpreted. We will find that buckling phenomena may be grouped into classes according to the relative magnitude of certain polynomial coefficients in an effective potential, much like phase transitions within Landau theory.

A. Buckling driven by dilative layer strain

The free energy appropriate for a two-dimensional layered material is written in the Monge representation,

$$F=\int d\mathbf{R}\sqrt{1+\mathcal{U}_X^2}\left\{\frac{B}{2}\left[\frac{d(\mathbf{R})-d_{eq}}{d_{eq}}\right]^2+\frac{K}{2}\left(\frac{1}{\mathcal{R}(\mathbf{R})}\right)^2\right\}, \tag{1}$$

where $d(\mathbf{R})$ is the actual layer spacing as a function of $\mathbf{R}=(X,Z)$, d_{eq} is the equilibrium value, and $\mathcal{R}(\mathbf{R})$ is the radius of curvature. Both these quantities can be expressed in terms of $\mathcal{U}(\mathbf{R})$, the deviation of the layers from their equilibrium positions:

$$\frac{d-d_{eq}}{d_{eq}}=\frac{1+\mathcal{U}_Z-\sqrt{1+\mathcal{U}_X^2}}{\sqrt{1+\mathcal{U}_X^2}}, \tag{2}$$

$$\frac{1}{\mathcal{R}}=\frac{\mathcal{U}_{XX}}{(1+\mathcal{U}_X^2)^{3/2}}. \tag{3}$$

We suppose that the layers are uniformly dilated in the Z direction, ignore boundary effects, and suppose that the buckling pattern is independent of z,

$$\mathcal{U}(\mathbf{R})=\alpha Z+u(X), \tag{4}$$

restrictions which are all removed in later sections of this work. Plugging Eqs. (2)–(4) into Eq. (1), and setting the functional derivative with respect to $u(X)$ to zero, we obtain a one-dimensional equation satisfied by $w(X)\equiv u_X(X)$ (thin solid curves in Fig. 3):

$$w_{xx}=\frac{1}{2}w(1+w^2)(w^2-\alpha(\alpha+2))+\frac{5}{2}\left(\frac{ww_x^2}{1+w^2}\right). \tag{5}$$

In the preceding equation, we used $X=\lambda x=\sqrt{K/B}x$, where λ is the usual penetration depth, to remove explicit dependence on the elastic constants from the equation.

For small $\mathcal{U}_X$, we can neglect the metric $\sqrt{1+\mathcal{U}_X^2}$ in Eq. (1), and take only leading powers of $\mathcal{U}$ in Eq. (2) and (3). Using uniform dilation [Eq. (4)], we obtain a simplified free energy

$$F\approx\int d\mathbf{R}\left\{\frac{B}{2}\left(\alpha-\frac{1}{2}w^2\right)^2+\frac{K}{2}w_X^2\right\}, \tag{6}$$

which, when minimized, yields the following approximate analog to Eq. (5):

$$w_{xx}=\frac{1}{2}w(w^2-2\alpha). \tag{7}$$

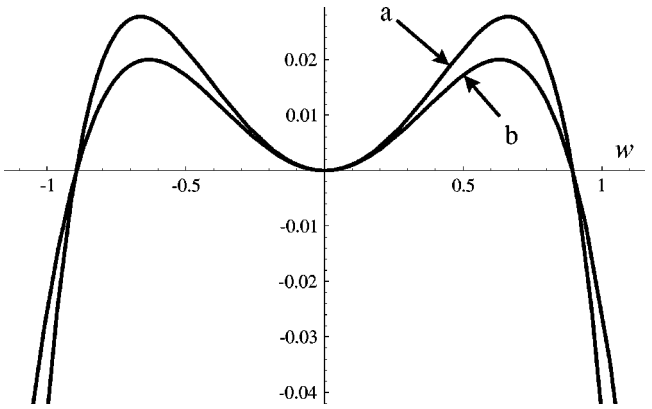

FIG. 2. Effective potentials in a mechanical analogy for the equations governing layer buckling. (a) Full equations (5) or (9). (b) Approximate equations (7) or (8). Functions are drawn for the dilative strain $\alpha=0.2$.

This approximation is used in later sections of this work, where boundary conditions in the Z direction and three-dimensional buckling situations are tackled. Equation (7) admits a closed form solution in terms of Jacobi θ functions [19] (thin dashed curves in Fig. 3), as described in Sec. III B.

There is a simple mechanical analogy [19] that explains how periodic solutions to Eq. (5), or its approximate form [Eq. (7)], arise. Considering x to be a time variable, Eq. (7) is the equation for a classical trajectory in the inverted quartic well potential:

$$\frac{\alpha}{2}w^2-\frac{1}{8}w^4. \tag{8}$$

The first term on the right of the exact equation (5) is, in the mechanical analogy, the force arising from the potential

$$\frac{\alpha}{2}\left(1+\frac{\alpha}{2}\right)w^2-\frac{1}{8}(1-2\alpha-\alpha^2)w^4-\frac{1}{12}w^6. \tag{9}$$

The potentials in Eqs. (8) and (9) have similar qualitative forms, as shown in Fig. 2.

Of the two boundary conditions needed to specify the solution of the second order differential equations (5) or (7), one controls the phase of the periodic solution and is not important unless boundary conditions in the x direction are invoked. The other may be pictured, in the mechanical analogy, as the energy of a particle. For small energies, the particle executes harmonic motion. Therefore, $w(x)$ $[=u_x(x)]$, and also its integral $u(x)$, are both sinusoidal functions (Fig. 3). The period of classical motion, and hence the stripe buckling wavelength, lengthens with increasing energy in the mechanical analogy. For large particle energies, the particle spends most of its time just inside the two maxima shown in Fig. 2. As a result, the solutions $w(x)$ acquire a square wave character, the flat portions arising as the particle lingers at the turning points located just inside the potential maxima in the mechanical analogy. Since flat portions of $w(x)$ are regions of constant slope in $u(x)$, the square wave limit of $w(x)$ implies that $u(x)$ appears like a zigzag or chevron. The ''velocity dependent'' term in Eq. (5) is seen in Fig. 3 to have only slight effect on the buckling profiles.

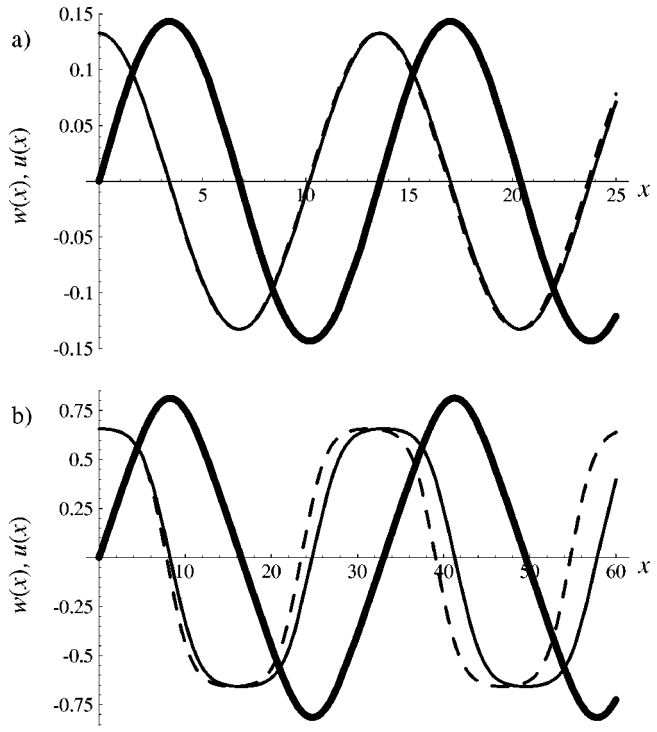

FIG. 3. Optimum buckling profile derivatives $w(x)=u_x(x)$, calculated using either the full equation (5), shown by the thin solid curves, or Eq. (7), with neglect of ''velocity'' dependent (i.e., w_x dependent) terms, as shown by the thin dashed curves. Functions are drawn for the dilative strain $\alpha=0.2$. As explained in the text, the character of the buckling profiles is controlled by the particle energy in the mechanical analogy. The particle energy equals (a) 25% or (b) 99% of the barrier height in Fig. 2. From the different scales of the axes, note that the buckling wavelength increases with the particle energy. The thick solid curve is the integrated buckling profile $u(x)$, including the w_x dependent terms in Eq. (5), scaled by either (a) 0.2 or (b) 0.5 to fit on the same plot with $w(x)$.

B. Comparison with surface area driven buckling

Membranes and Langmuir monolayers can buckle in response to compression, or coupling of composition and spontaneous curvature in multicomponent systems [36–38]. For the qualitative purposes of this section, we will examine the simplest case of one-dimensional buckling as treated by Milner, Joanny and Pincus [36]. The effective free energy, analogous to Eq. (1) in the case of layer strain, is

$$F=\int d\mathbf{R}\sqrt{1+\mathcal{U}_X^2}\left\{\sigma+\frac{K}{2}\left(\frac{1}{\mathcal{R}(\mathbf{R})}\right)^2\right\}, \tag{10}$$

where σ measures the compressive pressure on the membrane or monolayer, and $\mathcal{R}(\mathbf{R})$ is defined in Eq. (3). Buckling is induced when $\sigma<0$. At this stage, the effect of gravity is neglected.

With the substitution $\mathcal{U}_X(X)=w(x)$, where $X=\sqrt{K/(-\sigma)}x$ (recall that buckling occurs for $\sigma<0$), the Euler equation for the minimum energy profile becomes

$$w_{xx}=-w(1+w^2)^2+\frac{5}{2}\left(\frac{ww_x^2}{1+w^2}\right). \tag{11}$$

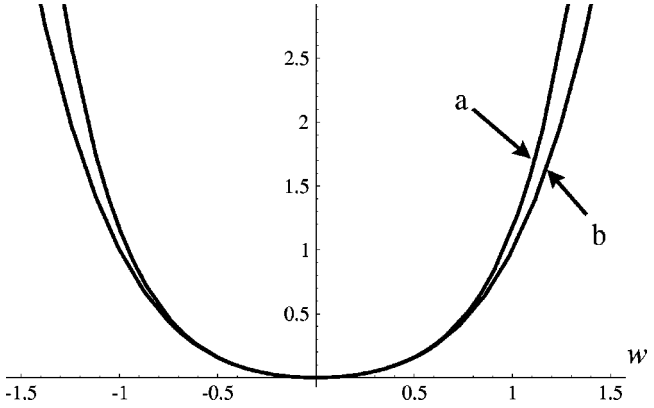

FIG. 4. Effective potentials in a mechanical analogy for the equations governing compression-induced monolayer or membrane buckling. (a) Full equations (11) or (9). (b) Approximate equations (13) or (14).

Just as in the case of layer strain-induced buckling, the above equation can be interpreted in a classical analogy as the motion of a particle. The qualitative behavior of the analogous particle is dominated by the potential

$$\frac{1}{6}[(1+w^2)^3-1], \tag{12}$$

which arises from the first term on the right of Eq. (11).

The potential function in the mechanical analogy for compression-induced monolayer or membrane buckling, Eq. (12) or Fig. 4, increases monotonically away from the origin, and is qualitatively different from that of Eq. (2) for dilative strain-induced layer buckling. Consequently, beyond the harmonic limit (small energy in the mechanical analogy), the character of the buckling patterns are also qualitatively different. For compression-induced monolayer buckling, the particle is rapidly accelerated from its turning points, unlike the case of strain-induced layer buckling, where the particle experiences little acceleration near the potential maxima of Fig. 2. Consequently the *derivative* function $w(x)$ $(=u_X)$ for compression-induced buckling approaches a zigzag or chevron shape, as shown in Fig. 5, not the buckling pattern itself as for strain-induced layer buckling. The slope of the zigzag pattern is diminished near $w(x)=0$, the region of maximum velocity, by the ''velocity'' dependent term in Eq. (11) whose action opposes that of the first term. (Compare the solid and dashed thin lines of Fig. 5). With increasing energy, the compression-induced buckling pattern itself becomes *more* rounded than the sinusoidal, low-energy limit, in contrast to the dilative strain-induced layer buckling.

The effective potential for compression-induced buckling (Fig. 4) increases more rapidly than a harmonic potential as one moves away from the origin, unlike the effective potential for dilative strain-induced buckling. This feature of the mechanical analogy explains why the compression-induced buckling wavelength *decreases* as one moves away from the harmonic limit, in contrast to dilative strain-induced buckling. Of course, this behavior is to be expected from monolayers or membranes under compression.

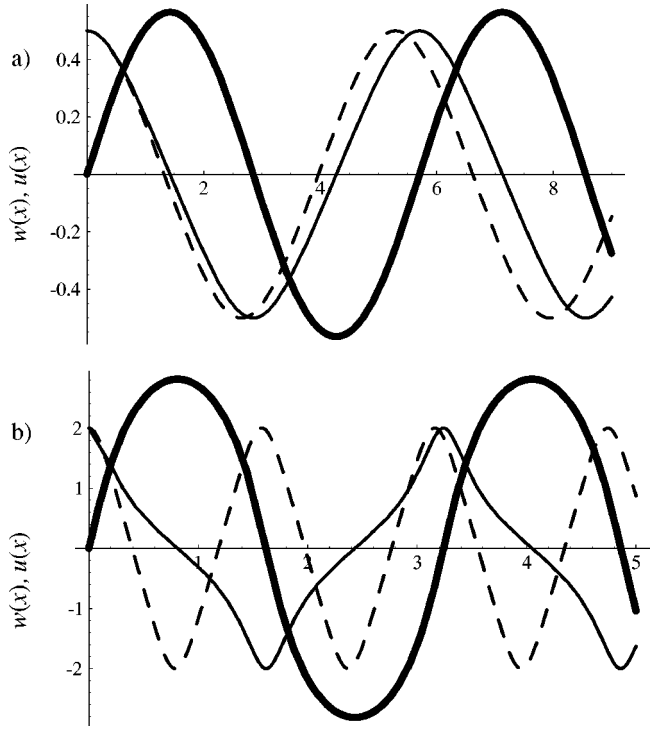

FIG. 5. Optimum buckling profile derivatives $w(x)=u_x(x)$ calculated using either the full equation (11), shown by the thin solid curves, or Eq. (13) with neglect of the ''velocity'' dependent (i.e., w_x dependent) terms, as shown by the thin dashed curves. As explained in the text, the character of the buckling profiles is controlled by the particle energy in the mechanical analogy. The particle energy equals (a) 0.5 or (b) 2.0. Note that the buckling wavelength decreases with particle energy. The thick solid curve is the integrated buckling profile $u(x)$, scaled by either (a) 1.3 or (b) 2 to fit on the same plot with $w(x)$.

An appropriate approximation of Eqs. (11) and (12) is obtained by dropping the velocity dependent term in Eq. (11) and the highest order term in potential (12). The resulting equation

$$w_{xx}=-w(1+2w^2) \tag{13}$$

is that of a particle moving in the potential:

$$\frac{1}{2}(w^2+w^4). \tag{14}$$

The qualitative difference from the layer strain case is the difference in sign of the quartic term. Equations (13) and (14) also admit a closed form solution in terms of Jacobi theta functions [39].

II. REDUCED FREE ENERGY FOR BUCKLING INDUCED BY DILATIVE LAYER STRAIN

Using the results of Sec. I as a guide, we now consider dilative strain-induced layer buckling on a quantitative level for either two- or three-dimensional layered materials, including smectic-*A* liquid crystals. The *Z* direction is perpendicular to the smectic layers. The smectic free energy, appropriate for small distortions [corresponding to the approximate forms (7) and (8) above], is

$$F=\int d\mathbf{R}\left\{\frac{B}{2}\left[\mathcal{U}_Z-\frac{1}{2}(\mathcal{U}_X^2+\mathcal{U}_Y^2)\right]^2+\frac{K}{2}(\mathcal{U}_{XX}+\mathcal{U}_{YY})^2\right\}. \tag{15}$$

The integration over $\mathbf{R}$ extends between $\pm L_x/2$ in the x direction, $\pm L_y/2$ in the y direction, and $\pm L_z/2$ in the z direction. Inclusion of the first derivative term proportional to $(\mathcal{U}_X^2+\mathcal{U}_Y^2)$ in the compression and/or dilation energy is essential to describe the transition from sinusoidal to chevron buckling patterns as strain is increased beyond the threshold value. Physically, this term, missing in the work of Stewart [32], ''informs'' the free energy that dilation followed by tilting can return the system to equilibrium, as discussed in the introduction.

The material is uniformly strained in the z direction. Express the displacement field as

$$\mathcal{U}(X,Y,Z)=\alpha Z+\lambda u(X,Y,Z)\equiv\frac{\lambda}{L_z}\overline{\alpha}Z+\lambda u(X,Y,Z), \tag{16}$$

where $\lambda=\sqrt{K/B}$ is the usual penetration depth, and the above equation serves to define a scaled strain $\overline{\alpha}\equiv(L_z/\lambda)\alpha$.

In terms of the reduced distances,

$$x\equiv\frac{\alpha^{1/2}}{\lambda}X,\quad y\equiv\frac{\alpha^{1/2}}{\lambda}Y\quad\text{and}\quad z\equiv\frac{Z}{L_z}, \tag{17}$$

the smectic free energy takes the form

$$F=\frac{B\lambda^3}{\overline{\alpha}}\int d\mathbf{r}\left\{\frac{1}{2}\left[\overline{\alpha}+u_z-\frac{\overline{\alpha}}{2}(u_x^2+u_y^2)\right]^2+\frac{\overline{\alpha}^2}{2}(u_{xx}+u_{yy})^2\right\}. \tag{18}$$

The integration over the scaled coordinate z extends between $\pm\frac{1}{2}$. Assuming a semi-infinite system in the x and y directions, the reduced layer profile $u(\mathbf{r})$ depends only on the dimensionless scaled strain $\overline{\alpha}$.

III. SEPARATION OF THE DISPLACEMENT FIELD AND THE z-PROFILE, $\phi(z)$

A. Factorization of the displacement field

To make further progress, we approximate the displacement field $u(\mathbf{r})$ as a product:

$$u(\mathbf{r})\approx\psi(x,y)\phi(z). \tag{19}$$

Boundary conditions are enforced by requiring $\phi(\pm\frac{1}{2})=0$. Since the xy plane is a symmetry plane for our system, $\psi(x,y)$ should exhibit no bias toward positive or negative values. As a consequence, all odd powers of $\psi(x,y)$ will integrate to zero. Using these simplifying features, we find a reduced free energy density f is given as

$$f\equiv\frac{\overline{\alpha}}{\mathcal{A}\lambda^3 B}F\left(\frac{L_z}{\lambda}\right)^2=\frac{\overline{\alpha}^2}{2}+\frac{1}{2}\langle\phi_z^2\rangle\langle\psi^2\rangle+\frac{\overline{\alpha}^2}{2}\left[-\langle\phi^2\rangle\langle|\nabla\psi|^2\rangle+\frac{1}{4}\langle\phi^4\rangle\langle|\nabla\psi|^4\rangle+\langle\phi^2\rangle\times\langle(\nabla^2\psi)^2\rangle\right], \tag{20}$$

where $\mathcal{A}$ is the area of a unit cell of the periodically replicated buckling pattern, and the angle brackets denote averages over a unit cell for xy integrals or over the system size for z integrals. We condensed our expressions using ''∇'' to stand for *only* x and y derivatives of $\psi(x,y)$. For example, $\langle\phi^2\rangle\equiv(1/L_z)\int_{-L_z/2}^{L_z/2}dZ\,\phi^2(Z)=\int_{-1/2}^{1/2}dz\,\phi^2(z)$ and $\langle|\nabla\psi|^2\rangle\equiv(1/\mathcal{A})\int\int_{\mathcal{A}}dx\,dy\,(\psi_x^2+\psi_y^2)$.

The optimal z profile $\phi(z)$ is found by setting the functional derivative of f with respect to $\phi(z)$ equal to zero:

$$\langle\psi^2\rangle\frac{d^2\phi}{dz^2}=\overline{\alpha}^2[-\langle|\nabla\psi|^2\rangle+\langle(\nabla^2\psi)^2\rangle]\phi+\frac{\overline{\alpha}^2}{2}\langle|\nabla\psi|^4\rangle\phi^3. \tag{21}$$

As introduced in Sec. I, the above equation is isomorphic to the classical mechanical equation of motion for a particle in an inverted quartic double-well potential,

$$m\frac{d^2\phi}{dz^2}=-\frac{\partial}{\partial\phi}\left\{\frac{A}{2}\phi^2-B\phi^4\right\}, \tag{22}$$

where z in the buckling problem maps onto time in the classical analogy, the mass is the classical analogy is

$$m=\langle\psi^2\rangle, \tag{23}$$

the constants in the inverted quartic potential are

$$A=\overline{\alpha}^2[\langle|\nabla\psi|^2\rangle-\langle(\nabla^2\psi)^2\rangle], \tag{24}$$

$$B=\frac{\overline{\alpha}^2}{8}\langle|\nabla\psi|^4\rangle, \tag{25}$$

and the equation of motion is to be solved subject to

$$\phi\left(\pm\frac{1}{2}\right)=0. \tag{26}$$

This analogy with a classical mechanical problem was first observed in earlier work on layer buckling in two-dimensional systems [19], and is seen to carry over to higher dimensions in this work.

B. Standard solutions $p(s)$ to the Euler equation

Since differential equations like Eqs. (7), (21), and (22) will appear yet again in another context, it is convenient to specify $\phi(z)$ is terms of solutions $p(s|\epsilon)$ to a standard problem,

$$\frac{d^2p}{ds^2} = -\frac{\partial}{\partial p}\{2p^2 - p^4\}, \tag{27}$$

where ϵ is the energy of the particle in the standard situation. The choice of this standard is arbitrary, although convenient since the peaks of the potential $V(p) = 2p^2 - p^4$ occur at $p = \pm 1$, and the value of the potential at the peaks is also equal to 1. With this choice, only $0 \leqslant \epsilon < 1$ could lead to solutions of physical interest. Further restrictions on ϵ will also apply, and lead to the threshold condition for buckling.

By straightforward coordinate transformation $\phi(z)$ is given in terms of solutions to the standard problem, $p(s|\epsilon)$:

$$\phi(z) = \frac{1}{2}\left(\frac{A}{B}\right)^{1/2} p(s|\epsilon), \tag{28}$$

$$z = 2\left(\frac{m}{A}\right)^{1/2} s - z_0. \tag{29}$$

The parameters z_0 and ϵ will be chosen to satisfy the boundary condition (26). The energy E of the particle in the classical analogy of Eq. (22), before transformation to the standard problem, is related to ϵ by

$$E = \frac{A^2}{16B}\epsilon. \tag{30}$$

The standard trajectories $p(s|\epsilon)$ admit an analytic solution. They are given implicitly in terms of $F(\theta|m)$, elliptic integrals of the first kind [40]:

$$s = (2\zeta_+)^{-1/2} F\left(\theta \middle| \frac{\zeta_-}{\zeta_+}\right), \tag{31}$$

$$\zeta_\pm = 1 \pm (1-\epsilon)^{1/2}, \tag{32}$$

$$\sin\theta = \zeta_-^{-1/2} p. \tag{33}$$

The period of motion is

$$\tau(\epsilon) = 2^{3/2}\zeta_+^{-1/2} K\left(\frac{\zeta_-}{\zeta_+}\right), \tag{34}$$

where $K(m)$ is the complete elliptic integral of the first kind [40]. The trajectories are also given explicitly in terms of Jacobi elliptic functions [40]:

$$p(s|\epsilon) = \sqrt{\zeta_-}\,\mathrm{sn}(\sqrt{2\zeta_+}s|m), \quad m \equiv \frac{\zeta_-}{\zeta_+}. \tag{35}$$

C. Threshold condition

Definition (31) and the periodicity of the trajectories imply that $p(0|\epsilon) = p([\tau(\epsilon)/2]|\epsilon) = 0$. Furthermore, $p(s|\epsilon) > 0$ in the range $0 < s < \tau(\epsilon)/2$. Therefore, the boundary condition $\phi(-\frac{1}{2}) = 0$ is satisfied by choosing $z_0 = \frac{1}{2}$ in Eq. (29). The boundary condition $\phi(\frac{1}{2}) = 0$ is satisfied by choosing ϵ to be the special value, here denoted "ϵ_z," for which (by substitution of $z = \frac{1}{2}$, $z_0 = \frac{1}{2}$, and $s = [\tau(\epsilon_z)/2]$ into Eq. (29)),

$$\tau(\epsilon_z) = \left(\frac{A}{m}\right)^{1/2} = \overline{\alpha}[\langle|\nabla\psi|^2\rangle - \langle(\nabla^2\psi)^2\rangle]^{1/2}\langle\psi^2\rangle^{-1/2}. \tag{36}$$

In the limit of small ϵ, $\tau(\epsilon) = \pi + (3\pi\epsilon/16) + O(\epsilon^2)$. With increasing ϵ, $\tau(\epsilon)$ increases monotonically. As ϵ approaches 1, $\tau(\epsilon)$ diverges logarithmically. The lower limit on $\tau(\epsilon_z)$ provides a threshold condition for layer buckling. This can be seen by taking $\psi(x,y)$ to be the linear combination,

$$\psi(x,y) \approx \sum_n C_n e^{i\mathbf{k}_n\cdot\mathbf{r}}, \tag{37}$$

where $\mathbf{k}_n$ are members of a finite set of reciprocal lattice vectors from a two-dimensional lattice. Inserting the limiting form of $\psi(x,y)$ into Eq. (36), we find

$$\tau(\epsilon_z) = \overline{\alpha}\left[\sum_n |C_n|^2(|\mathbf{k}_n|^2 - |\mathbf{k}_n|^4)\right]^{1/2}\left(\sum_n |C_n|^2\right)^{-1/2}. \tag{38}$$

Since $\tau(\epsilon_z) \geqslant \pi$, the right hand side of the preceding equation must be greater than or equal to π to satisfy boundary conditions (26). To determine threshold conditions, we seek the wave vectors $\mathbf{k}_n$ which make the right hand side of Eq. (38) as large as possible. The magnitudes of $\mathbf{k}_n$ are easily found to be

$$|\mathbf{k}_n| = 2^{-1/2}. \tag{39}$$

At these wave vectors, the right hand side of Eq. (38) is independent of C_n, and equal to $\overline{\alpha}/2$, which must be greater than the threshold value of π:

$$\overline{\alpha} \geqslant 2\pi. \tag{40}$$

Recalling the definition of reduced units in Sec. II, this is in agreement with previous derivations of the threshold condition [21,25]. Combining Eqs. (28) and (29) with properties (38)–(40) at threshold, we obtain, for future reference, the z profile at threshold:

$$\phi(z) = \frac{1}{4}\left(\frac{A}{B}\epsilon_z\right)^{1/2}\cos(\pi z) \quad \text{(threshold)}. \tag{41}$$

D. Form of the free energy with the optimum z profile

Henceforth the z profile $\phi(z)$ will be regarded as a functional of the xy profile, as specified in Eqs. (23)–(25) and (28). The reduced free energy f given in Eq. (20) takes a simpler form when the explicit dependence of the optimum $\phi(z)$ on $\psi(x,y)$ is taken into account.

The ϕ_z^2 term in the free energy can be removed using the analog to the conservation of energy in Eq. (22), which is isomorphic to a classical equation of motion:

$$\frac{1}{2}m\left(\frac{d\phi}{dz}\right)^2 + \frac{A}{2}\phi^2 - B\phi^4 = E = \frac{A^2}{16B}\epsilon_z. \tag{42}$$

The last equality follows upon comparison with the standard problem (28) for which $\frac{1}{2}(dp/ds)^2 + 2p^2 - p^4 = \epsilon$.

The fourth moment of the z profile, $\langle \phi^4 \rangle = \frac{1}{16} A^2/B^2 \langle p^4 \rangle$, can be related to the second moment using a standard identity from the theory of Jacobian elliptic functions [41]. In terms of the standard solutions, this identity reads

$$\langle p^4 \rangle = \frac{4}{3}\langle p^2 \rangle - \frac{1}{3}\epsilon_z . \tag{43}$$

Substituting Eqs. (42) and (43) into expression (20) for the free energy, we obtain

$$f = \frac{\overline{\alpha}^2}{2} + \frac{\overline{\alpha}^2}{6}\frac{(\langle |\nabla \psi|^2 \rangle - \langle (\nabla^2 \psi)^2 \rangle)^2}{\langle |\nabla \psi|^4 \rangle}(\epsilon_z - 4\langle p^2 \rangle_{\epsilon_z}). \tag{44}$$

IV. XY PROFILE, $\psi(X,Y)$, AND MIDSAMPLE BUCKLING PATTERN

Since A,B, and m in Eq. (22) depend on the xy profile $\psi(x,y)$, the optimum z profile is a functional of the xy profile: $\phi = \phi[\psi(x,y)]$. Under the ansatz of Eq. (19) the free energy can be regarded as a functional of the xy profile, $f[\psi,\phi] = f[\psi,\phi[\psi]]$, and could conceivably be directly minimized with respect to ψ. However, a further approximation results in a less cumbersome procedure which involves minimization over just a few parameters. We isolate a portion of the free energy f of Eq. (20), identified as g in the following equation, which governs the behavior of the xy buckling pattern ψ away from the boundaries at $z = \pm \frac{1}{2}$:

$$f = \frac{\overline{\alpha}^2}{2} + \frac{1}{2}\langle \phi_z^2 \rangle \langle \psi^2 \rangle + \frac{\overline{\alpha}^2}{2}\langle \phi^2 \rangle g\left[\psi \middle| \frac{\langle \phi^4 \rangle}{\langle \phi^2 \rangle} \right], \tag{45}$$

$$g[\psi|\gamma] \equiv -\langle |\nabla \psi|^2 \rangle + \frac{\gamma}{4}\langle |\nabla \psi|^4 \rangle + \langle (\nabla^2 \psi)^2 \rangle. \tag{46}$$

When the z coordinate is not too close to the system boundaries at $z = \pm \frac{1}{2}$, we expect the buckling pattern to be relatively independent of the z coordinate. If the z variation of the buckling profile is neglected, minimization of the free energy reduces to a minimization of g, regardless of whether the buckling profile is approximately factored into a product of xy and z parts as in Eq. (19). This is easily seen by letting $u_z \to 0$ in Eq. (18).

We will soon find that γ in Eq. (46) only affects the normalization of ψ. To within that normalization, the buckling profiles ψ that minimize g only depend upon the unit cell size and shape chosen for the buckling pattern. (The free energy is subsequently minimized with respect to the unit cell dimensions.) Hence we need only consider profiles $\tilde{\psi}$ that optimize a functional $\tilde{g}$, which is defined below to be the functional g, where γ is set to a conventional value which we arbitrarily take to be unity. This is expected on physical grounds, since γ depends only on ϕ, and for a slowly varying z profile ϕ only contains information on the normalization of the buckling pattern. Hence the value of γ should not affect the *shape* of the profile $\tilde{\psi}$.

Demonstrating that γ does not affect the shape of $\tilde{\psi}$ is achieved with the substitution

$$\psi(x,y) = \gamma^{-1/2}\tilde{\psi}(x,y) \tag{47}$$

in Eq. (46). With that substitution, we find that

$$g[\psi|\gamma] = \gamma^{-1} g[\tilde{\psi}|1] \equiv \gamma^{-1}\tilde{g}[\tilde{\psi}]. \tag{48}$$

Hence the optimal pattern $\tilde{\psi}$ with γ set equal to unity is related to the optimal buckling profile with any other fixed normalization by transformation (47). In all subsequent work, we work with the scaled xy profile $\tilde{\psi}$, in effect adopting a standard normalization for $\psi(x,y)$. Of course, the normalization of ψ is arbitrary, although that of the complete buckling profile $\phi(z)\psi(x,y)$ is not. While the functional $\tilde{g}$ has no explicit dependence on any parameters, boundary conditions in the form of specifying a wavelength for the periodic functions $\tilde{\psi}$ will introduce a free parameter for each modulation direction.

To gain further insight and simplicity, we do not pursue the straightforward approach of numerically optimizing Eq. (20) or (44) while self-consistently allowing for the depedence of the optimum ϕ on ψ. Instead, we restrict the variation of ψ to the family of solutions $\tilde{\psi}$ obtained by minimizing g in Eq. (46) with variable boundary conditions and variable scaling factors, as parametrized by q_x and q_y, in the x and y directions:

$$\psi(x,y) \approx \tilde{\psi}(q_x x, q_y y). \tag{49}$$

This is a considerable simplification because, for a fixed unit cell geometry, this leads to a low-dimensional minimization, turning the minimization of f into a search over just two parameters for each independent direction of modulation. For a one-dimensional buckling pattern, or, for example, for a square buckling pattern for which we expect $q_x = q_y$, the optimization is over only two parameters. This approximation was already shown to reproduce all qualitative features of experiments involving single-wave vector buckling patterns [12–16], and was successfully put to a quantitative test in some instances [18,20].

V. RESULTS

Buckling patterns along both one and two directions are observed in smectic-A materials subjected to dilative strain [1]. We treated the single-wave vector case in previous work [19], but it is useful to briefly review and extend these results here before proceeding to the full three-dimensional case. The previous results are further simplifed in this work.

A. Unidirectional buckling pattern

If layers are modulated along a single direction, taken as the x direction, the limiting expression for $\tilde{g}[\tilde{\psi}]$

$$\tilde{g}[\tilde{\psi}] = -\langle (\tilde{\psi}_x)^2 \rangle + \frac{1}{4}\langle (\tilde{\psi}_x)^4 \rangle + \langle (\tilde{\psi})_{xx}^2 \rangle \tag{50}$$

is minimized when $\tilde{\psi}$ satisfies

$$\tilde{\psi}_{xxx} = -\tilde{\psi}_x + \frac{1}{2}(\tilde{\psi}_x)^3. \tag{51}$$

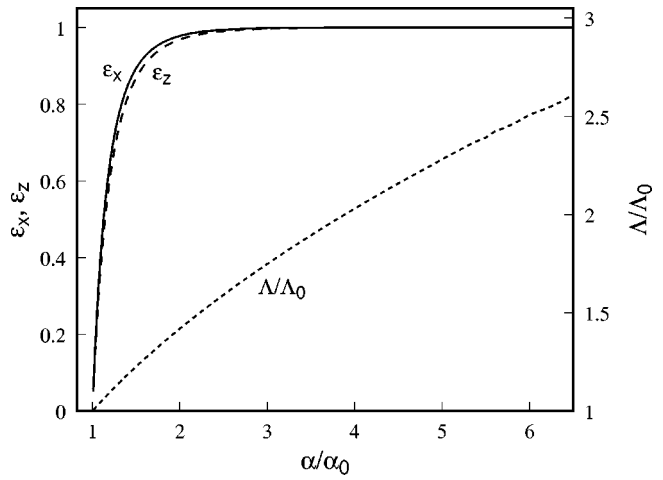

FIG. 6. Parameters ϵ_x (solid line), ϵ_z (long dashed line), and wavelength $\Lambda = 2\pi(\epsilon_x)/q_x$ (short dashed line) of the optimal pattern for two-dimensional buckling as a function of strain α. Strain is given relative to the threshold value of $\alpha_0 = 2\pi\lambda/L_z$. The buckling wavelength is relative to the threshold value of $\Lambda_0 = \sqrt{4\pi L_z \lambda}$. ϵ_x and q_x parametrize $\tilde{\psi}(q_x x)$ as given in Eqs. (49) and (54). ϵ_z is regarded as a functional of the buckling profile in the x direction, as in Eq. (36).

Setting $w = \tilde{\psi}_x$, we find that w satisfies

$$w_{xx} = -\frac{\partial}{\partial w}\left[\frac{w^2}{2} - \frac{w^4}{8}\right], \tag{52}$$

which is precisely of the same form as Eq. (22), the equation of motion in an inverted double-well potential. (See the discussion of Sec. I.) Therefore, the optimum single-wave vector buckling patterns are

$$w(x) = \sqrt{2}\, p(s|\epsilon_x), \quad s = \frac{1}{2}x, \tag{53}$$

where $p(s|\epsilon_x)$ is defined in Eqs. (31)–(35). The actual buckling pattern is obtained by integrating the above equation,

$$\tilde{\psi}(x) = 2\ln\left[\frac{\mathrm{dn}(\sqrt{2\zeta_+}s|m) - \sqrt{m}\,\mathrm{cn}(\sqrt{2\zeta_+}s|m)}{\sqrt{1-m}}\right], \tag{54}$$

where $s = \frac{1}{2}x$, $m = \zeta_-/\zeta_+$, and $\zeta_\pm = 1 \pm \sqrt{1-\epsilon_x}$. The parameter ϵ_x controls the shape of the x-direction buckling profile, sinusoidal for small ϵ_x and chevrons for $\epsilon_x \to 1$. Just like the z- profile, the x-direction buckling pattern is related to the trajectory of a particle in an inverted double well, and ϵ_x is the scaled energy in the mechanical analogy. In the x- profile case, the integral of the trajectory with respect to time is the physically relevant quantity in the layer buckling problem. In the mechanical problem the parameter ϵ_x controls the period of motion, and hence in the buckling problem controls the buckling wavelength. The actual value of ϵ_x is determined by optimizing the full free energy expression, Eq. (20) or Eq. (44).

Results for optimizing f, as given in Eq. (44), are presented in Fig. 6. At threshold, ϵ_x and ϵ_z are both zero, and a single Fourier mode treatment is accurate. However, both these parameters rapidly increase to unity with increasing strain, and the buckling pattern must be described by the full nonlinear theory. According to Eqs. (53) and (54), the wave length Λ of the buckling pattern in the reduced distance x is

$$\Lambda = \frac{2\pi(\epsilon_x)}{q_x}, \tag{55}$$

and is shown in Fig. 6 to increase steadily with increasing strain. [To obtain a physical length, the above expression for Λ should be multiplied by $\lambda/\alpha^{1/2}$, as specified in Eq. (17).] The behavior of our calculated Λ explains why buckled stripe domains in a thin magnetic film are observed to have an increasing zigzag wavelength with increasing dilative strain [13,14].

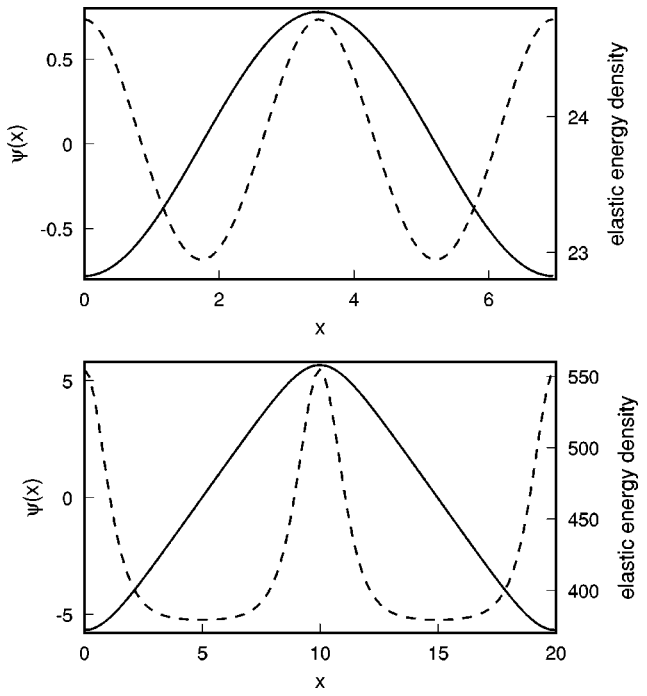

FIG. 7. Buckling profile (solid line) and elastic energy density (dashed line) for layer buckling in a two-dimensional system for strain $\alpha/\alpha_0 = 1.1$ (top panel) and $\alpha/\alpha_0 = 5.0$. Strain is given relative to the threshold value of $\alpha_0 = 2\pi\lambda/L_z$. The elastic energy density is the integrand in Eq. (20) evaluated at $z = 0$. With increasing strain, the buckling pattern changes from sinusoidal to zigzag in nature, and the elastic energy density becomes concentrated near the corners of the zigzag pattern.

The nature of the buckling profiles in a two-dimensional system is depicted in Fig. 7. The pattern evolves from sinusoidal to zigzig, in character with increasing strain. Also shown in Fig. 7 is the elastic energy density, the integrand in Eq. (20), plotted for $z = 0$ at the middle of the sample. The elastic energy steadily concentrates near the kinks of the buckling profile in the zigzag limit.

B. Modulation of the buckling pattern in two directions

We have obtained optimal buckling patterns, modulated in two directions, beyond the single wave vector limit, by expanding $\tilde{\psi}(x,y)$ in a Fourier series. Since Delrieu showed that at threshold the triangular buckling pattern is higher in energy than one with two orthogonal wave vectors [25], we confine our attention to rectangular patterns. First, buckling

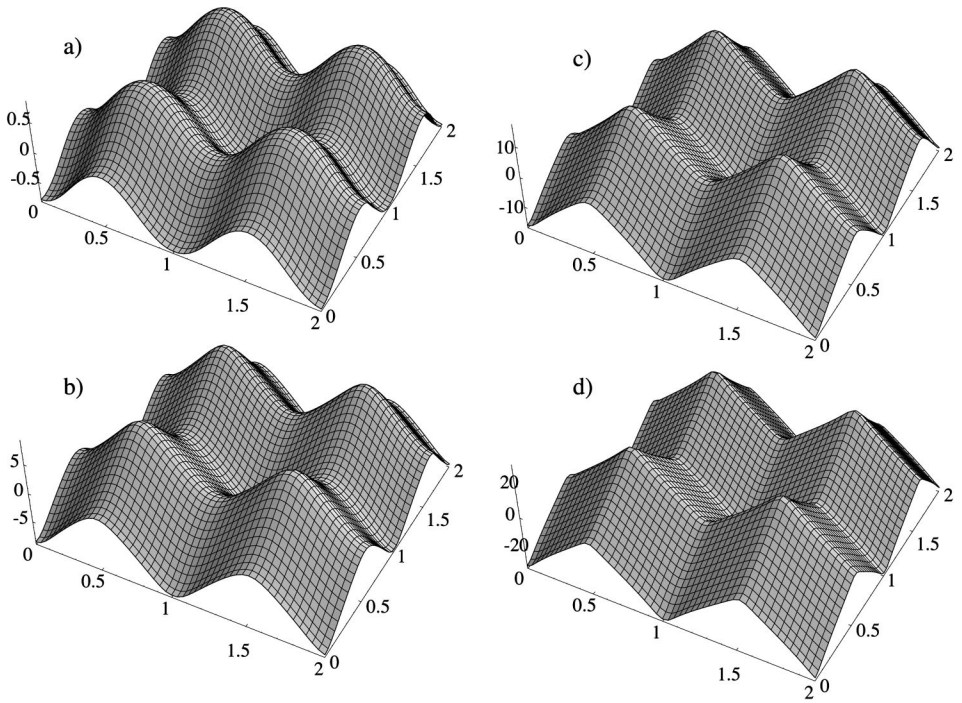

FIG. 8. Buckling patterns $\tilde{\psi}$ which minimize the free energy $\tilde{g}$ defined in Eqs. (45)–(48). The patterns are calculated for different boundary conditions as determined by l the length of the square unit cell: $(l/2\pi)^2=$ (a) 1.1, (b) 10, (c) 30, and (d) 100. The independent variables are x/l and y/l, and a total of four periodic cells are shown in each case. Buckling pattern (a) is optimum for a strain $\alpha/\alpha_0 \approx 1.5$, pattern (b) is optimum for strain of $\alpha/\alpha_0 \approx 5.9$, and patterns (c) and (d) are observed for strain values of $\alpha/\alpha_0 > 20$. (α_0 is the threshold value of strain, $2\pi\lambda/L_z$.) With increasing strain, the buckling pattern evolves in a manner that reflects the change from sinusoidal to zigzag in nature, as seen in the two-dimensional buckling patterns of Fig. 7.

patterns that optimize the functional $\tilde{g}$ [Eq. (48)] are determined. This generates a family of solutions $\tilde{\psi}(x,y)$ indexed by a single parameter, the unit cell size l in the case of a square buckling pattern, or two parameters l_x and l_y for the general rectangular pattern. Samples of these solutions are presented in Fig. 8, illustrating the transition from sinusoidal to chevron character for the three-dimensional case. Just above threshold [$\alpha/\alpha_0=1.1$ in panel (a)], the buckling pattern is essentially a single Fourier mode in each orthogonal direction. With increasing wavelength l the buckling pattern evolves toward flat regions joined at creases.

Once the patterns which minimize the reduced functional $\tilde{g}$ are generated, a variational scale parameter q is inserted for each direction, $\tilde{\psi}(qx,qy)$ for square patterns or $\tilde{\psi}(q_x x,q_y y)$ for the general rectangular case, and the free energy f [Eq. (44)] is optimized with respect to two parameters l and q for a square lattice, and four parameters l_x, l_y, q_x, and q_y, for the general rectangular lattice. The parameters l or (l_x,l_y) control the nature of the buckling pattern, as did the parameter ϵ_x in the two-dimensional case. Shown in Fig. 9 is the buckling wavelength $\Lambda=l/q$ for a square buckling pattern as a function of strain. The optimal buckling pattern rapidly departs from the single mode solution as the strain rises above threshold. Likewise, the z-profile parameter ϵ_z rises steeply to unity with increasing strain, indicating the failure of the single-mode solution for $\phi(z)$ as well. The distribution of elastic energy, as measured by the integrand in Eq. (20) evaluated at $z=0$, is depicted in Fig. 10. The elastic energy tends to concentrate at apical points. We expect the flat regions of the buckling pattern to contain very little of the total elastic energy in the high strain limit. The fact that there is some residual elastic energy in the flat regions of the buckling pattern, as in the lower panel of Fig. 10, is partly due to small curvature at this level of strain, but partly reflects the fact that the buckling pattern is a mean field compromise for the entire sample, not just for

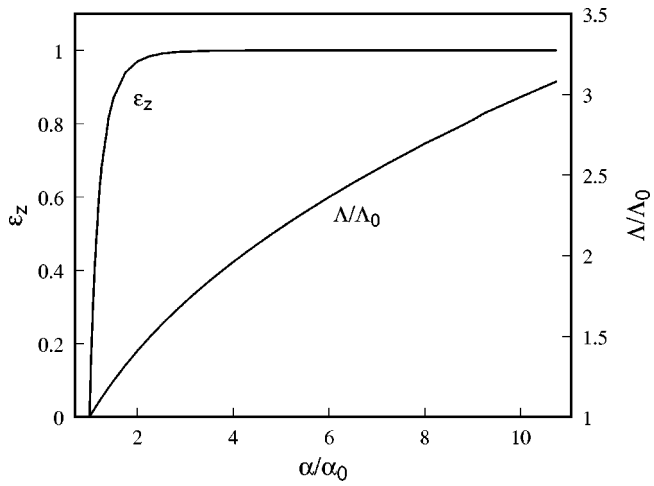

FIG. 9. Parameter ϵ_z and wavelength Λ of the optimal pattern for three-dimensional square buckling as a function of strain α. Strain is given relative to the threshold value of $\alpha_0=2\pi\lambda/L_z$. The buckling wavelength is relative to the threshold value of $\Lambda_0=\sqrt{4\pi L_z\lambda}$. ϵ_z is regarded as a functional of the buckling profile in the x- direction, as in Eq. (36).

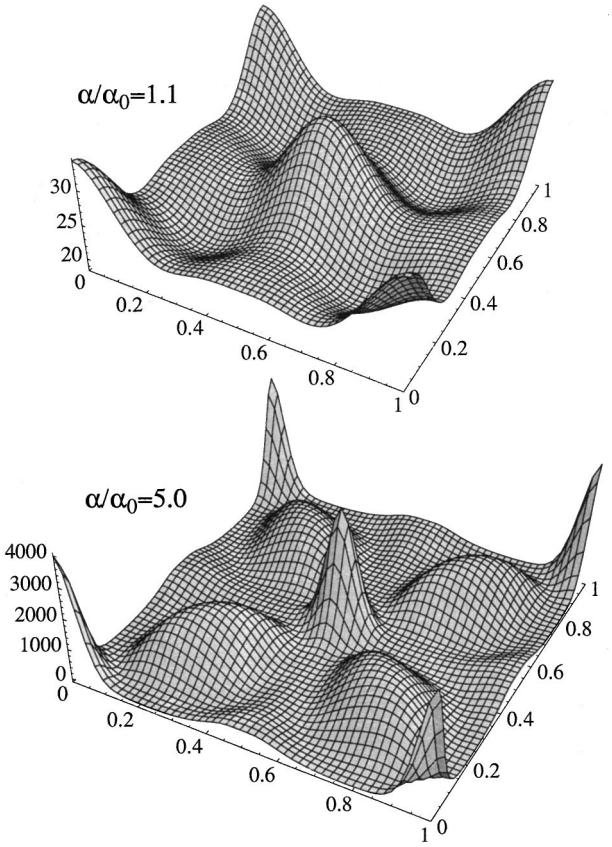

FIG. 10. Elastic energy density for layer buckling in a two-dimensional system for strain $\alpha/\alpha_0=1.1$ and 5.0. Strain is given relative to the threshold value of $\alpha_0=2\pi\lambda/L_z$. The elastic energy density is the integrand in Eq. (20) evaluated at $z=0$. The independent variables are x/l and y/l. The elastic energy density becomes concentrated near apical points with increasing strain.

$z=0$.

Buckling patterns modulated in both one and two directions are observed in experiments on smectic liquid crystals under dilative strain [1]. Near threshold, in the limit of a single Fourier mode for each direction, unidirectional and bidirectional solutions are exactly degenerate. The degeneracy is lifted, and the square pattern is favored with increasing strain and the appearance of higher Fourier modes (Fig. 11), accounting for the experimental observation that the square pattern emerges in smectics beyond threshold [1]. We have also calculated buckling patterns and overall energy for rectangular patterns. The rectangular patterns are intermediate in energy between the unidirectional modulation and square patterns, and are not shown here.

VI. DISCUSSION

Both a qualitative analysis and a calculation of dilative strain-induced buckling patterns are presented in this work. Our qualitative analysis, couched in terms of a mechanical analogy, suggests that layer buckling patterns are not universal. For example, the compression-induced interface modulation yields a profile in which the peaks become more rounded with increasing strain. This is just the opposite of dilative strain-induced buckling, where the profile turns into straight segments joined by kinks in the large strain limit.

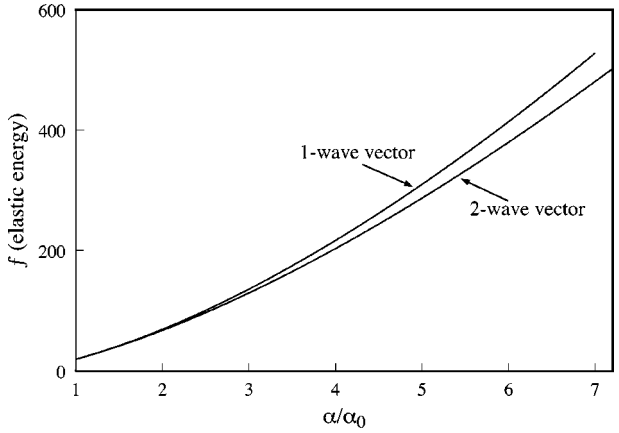

FIG. 11. Comparison of the elastic energy of layers buckling along a single direction, or two directions. They are degenerate in the single-mode limit, but the bidirectional solution with a square unit cell becomes lower in energy when nonlinear terms come into play. Solutions with a rectangular unit cell are intermediate in energy between the unidirectional and square buckling patterns.

Despite the lack of universality in the buckling pattern, both cases can be analyzed within the same analogy with a particle executing bound oscillations within a potential. The differences in buckling patterns are understood, within the mechanical analogy, in terms of qualitative features of the potential.

Even the three-dimensional profiles presented in Sec. V B may yet succumb to simple analytic forms. As can be seen in Fig. 8, the three-dimensional buckling profile approaches the function

$$\tilde{\psi}(x,y)\propto-\left(\frac{1}{2}-\left|\frac{2x}{l_x}\right|\right)-\left(\frac{1}{2}-\left|\frac{2y}{l_y}\right|\right),\quad\left(-\frac{1}{2}\leqslant\frac{x}{l_x},\frac{y}{l_y}\leqslant\frac{1}{2}\right) \tag{56}$$

within a unit cell centered at the origin, after which the pattern is periodically replicated. At threshold, the buckling profile is a sum of the lowest order Fourier modes:

$$\tilde{\psi}(x,y)=a_x\cos\left(\frac{2\pi x}{l_x}\right)+a_y\cos\left(\frac{2\pi y}{l_y}\right). \tag{57}$$

Since $\tilde{\psi}$ becomes of sum of a purely x-dependent function and a purely y-dependent function in the limit of both high and low dilative strain, this suggests that separation into a sum of x and y functions would be a fruitful area for future approximations, if desired.

Our calculated strain-induced buckling profile for stripes in thin films [13–15] or liquid crystals, modulated along a single direction [9–11], was previously calculated [19] and already compared with experiment [18,20]. In this work, we truly predict three-dimensional modulation patterns, that is, layer buckling modulated along more than one direction, which will hopefully be compared with experiment.

ACKNOWLEDGMENTS

Acknowledgement is made to the donors of The Petroleum Research Fund, administered by the ACS, for support of this research.

[1] R. Ribotta and G. Durand, J. Phys. (Paris) **38**, 179 (1977).
[2] Y. Ouchi, H. Takano, H. Takezoe, and A. Fukuda, Jpn. J. Appl. Phys., Part 1 **27**, 1 (1988).
[3] Y. Takanishi, Y. Ouchi, H. Takezoe, and A. Fukuda, Jpn. J. Appl. Phys., Part 2 **28**, L487 (1989).
[4] Y. Sato, T. Tanaka, H. Kobayashi, K. Aoki, H. Watanabe, H. Takeshita, Y. Ouchi, H. Takezoe, and A. Fukuda, Jpn. J. Appl. Phys., Part 2 **28**, L483 (1989).
[5] J. Fünfschilling and M. Schadt, Jpn. J. Appl. Phys., Part 1 **30**, 741 (1991).
[6] K. Itoh, M. Johno, Y. Takanishi, Y. Ouchi, H. Takezoe, and A. Fukuda, Jpn. J. Appl. Phys., Part 1 **30**, 735 (1991).
[7] N. Itoh, Y. Narutaki, T. Shinomiya, M. Koden, S. Miyoshi, and T. Wada, Jpn. J. Appl. Phys., Part 1 **31**, 1414 (1992).
[8] Y. Asao and T. Uchida, Jpn. J. Appl. Phys., Part 2 **32**, L604 (1993).
[9] G.P. Crawford, R.E. Geer, J. Naciri, R. Shashidhar, and B.R. Ratna, Appl. Phys. Lett. **65**, 2937 (1994).
[10] T.P. Rieker and N.A. Clark, in *Phase Transitions and Liquid Crystals*, Vol. 290 of *NATO Advanced Study Institute, Series B: Physics*, edited by S. Martellucci and A. N. Chester (Plenum, New York, 1992), Chap. 21, p. 287.
[11] A.G. Rappaport, P.A. Williams, B.N. Thomas, N.A. Clark, M.B. Ros, and D.M. Walba, Appl. Phys. Lett. **67**, 362 (1995).
[12] P. Molho, J. Gouzerh, J.C.S. Levy, and J.L. Porteseil, J. Magn. Magn. Mater. **54-57**, 857 (1986); P. Molho, J.L. Porteseil, Y. Souche, J. Gouzerh, and J.C.S. Levy, J. Appl. Phys. **61**, 4188 (1987).
[13] M. Seul and R. Wolfe, Phys. Rev. Lett. **68**, 2460 (1992).
[14] M. Seul and R. Wolfe, Phys. Rev. A **46**, 7519 (1992).
[15] M. Seul and R. Wolfe, Phys. Rev. A **46**, 7534 (1992).
[16] F. Elias, C. Flament, J.-C. Bacri, and S. Neveu, J. Phys. I **7**, 711 (1997).
[17] N.A. Clark and P.S. Pershan, Phys. Rev. Lett. **30**, 3 (1973).
[18] P. Oswald, J.C. Géminard, L. Lejcek, and L. Sallen, J. Phys. II **6**, 281 (1996).
[19] S.J. Singer, Phys. Rev. E **48**, 2796 (1993).
[20] R.E. Geer, S.J. Singer, J.V. Selinger, B.R. Ratna, and R. Shashidhar, Phys. Rev. E **57**, 3059 (1998).
[21] N.A. Clark and R.B. Meyer, Appl. Phys. Lett. **22**, 493 (1973).
[22] W. Helfrich, Appl. Phys. Lett. **17**, 531 (1970).
[23] W. Helfrich, J. Chem. Phys. **55**, 839 (1971).
[24] J.P. Hurault, J. Chem. Phys. **59**, 2068 (1973).
[25] J.M. Delrieu, J. Chem. Phys. **60**, 1081 (1974).
[26] Z.-G. Wang, J. Chem. Phys. **100**, 2298 (1994).
[27] M. Nakagawa, Displays **11**, 67 (1990).
[28] J. Pavel and M. Glogarova, Liq. Cryst. **9**, 87 (1991).
[29] L. Limat and J. Prost, Liq. Cryst. **13**(1), 101 (1993).
[30] S. Kralj and T.J. Sluckin, Phys. Rev. E **50**, 2940 (1994).
[31] N. Vaupotic, S. Kralj, M. Copic, and T.J. Sluckin, Phys. Rev. E **54**, 3783 (1996).
[32] I.W. Stewart, Phys. Rev. E **58**, 5926 (1998).
[33] H. Finkelmann, I. Kundler, E.M. Terentjev, and M. Warner, J. Phys. II **7**, 1059 (1997).
[34] J. Weilepp and H.R. Brand, Macromol. Theory Simul. **7**, 91 (1998).
[35] D.J. Read, R.A. Duckett, J. Sweeney, and T.C.B. McLeish, J. Phys. D **32**, 2087 (1999).
[36] S.T. Milner, J.-F. Joanny, and P. Pincus, Europhys. Lett. **9**, 495 (1989), AÈ.
[37] S. Leibler and D. Andelman, J. Phys. (Paris) **48**, 2013 (1987).
[38] J.-G. Hu and R. Granek, J. Phys. (France) **6**, 999 (1996).
[39] In analogy with the ''standard solution'' presented in Eqs. (27) and (35), the differential equation $d^2p/ds^2=-(\partial/\partial p)\{2p^2+p^4\}$ has an analytic solution $p(s)=\sqrt{\eta}\,\mathrm{cn}[2\sqrt{\delta}s|(\eta/2\delta)]$, where ϵ corresponds to the particle's energy in the classical analogy, $\delta=\sqrt{1+\epsilon}$, $\eta=\delta-1$, and cn is a Jacobi theta function [40].
[40] *Handbook of Mathematical Functions*, edited by M. Abramowitz and I.A. Stegun, (National Bureau of Standards, Applied Mathematics Series No. **55**, US, GPO, Washington, DC, 1972).
[41] E.H. Neville, *Jacobian Elliptic Functions* (Oxford University Press, New York, 1951), pp. 233 and 234.